The Journal of Chemical Physics ARTICLE scitation.org/journal/jcp

State dependent ring polymer molecular dynamics for investigating excited nonadiabatic dynamics

Cite as: J. Chem. Phys. 150, 244102 (2019); doi: 10.1063/1.5096276
Submitted: 15 March 2019 • Accepted: 3 June 2019 •
Published Online: 24 June 2019

Sutirtha N. Chowdhury and Pengfei Huo[a)]

AFFILIATIONS

Department of Chemistry, University of Rochester, 120 Trustee Road, Rochester, New York 14627, USA

Note: This paper is part of a JCP Special Topic on Dynamics of Open Quantum Systems.
[a)]**Electronic mail:** pengfei.huo@rochester.edu

ABSTRACT

A recently proposed nonadiabatic ring polymer molecular dynamics (NRPMD) approach has shown to provide accurate quantum dynamics by incorporating explicit state descriptions and nuclear quantizations. Here, we present a rigorous derivation of the NRPMD Hamiltonian and investigate its performance on simulating excited state nonadiabatic dynamics. Our derivation is based on the Meyer-Miller-Stock-Thoss mapping representation for electronic states and the ring-polymer path-integral description for nuclei, resulting in the same Hamiltonian proposed in the original NRPMD approach. In addition, we investigate the accuracy of using NRPMD to simulate the photoinduced nonadiabatic dynamics in simple model systems. These model calculations suggest that NRPMD can alleviate the zero-point energy leakage problem that is commonly encountered in the classical Wigner dynamics and provide accurate excited state nonadiabatic dynamics. This work provides a solid theoretical foundation of the promising NRPMD Hamiltonian and demonstrates the possibility of using the state-dependent RPMD approach to accurately simulate electronic nonadiabatic dynamics while explicitly quantizing nuclei.

I. INTRODUCTION

Open quantum systems, such as electronic states interacting with nuclear vibrations or the photon field, are ubiquitous in chemical physics. Accurately and efficiently simulating the quantum dynamics of the open subsystem with the influence from its environment (bath) remains one of the central challenges in theoretical chemistry[1,2] and condensed matter physics.[3] Directly performing exact quantum dynamics simulations for an open subsystem[4–10] or the closed system-bath total system is computationally demanding, despite exciting recent progress.[11–21] It is thus ideal to develop approximate methods that can accurately describe the open quantum dynamics of the subsystem (for example, nonadiabatic transitions among various electronic states) while treating the bath dynamics explicitly through classical-like trajectories.[1,2,22] To this end, a large number of these approaches are developed, including the popular trajectory surface-hopping method (mixed quantum-classical approach),[23–26] the semiclassical path-integral approaches,[22,27–33] the mixed quantum-classical Liouville (MQCL) equation,[2,34–37] the symmetrical quasiclassical (SQC) approach,[38–42] and the generalized quantum master equation (GQME).[43–47] Despite providing accurate electronic nonadiabatic dynamics, these approaches generally do not preserve quantum Boltzmann distribution (QBD)[48,49] or zero point energy (ZPE) associated with the nuclear degrees of freedom (DOF). They often suffer from numerical issues such as ZPE leakage,[50,51] although significant improvements are accomplished through the recent development.[38,45–47]

Imaginary-time path-integral approaches,[52–54] such as the centroid molecular dynamics (CMD)[55,56] and the ring-polymer molecular dynamics (RPMD),[57,58] resemble classical MD in an extended phase space and provide a convenient way to compute approximate quantum time-correlation functions.[57] The classical evolution of RPMD preserves its initial quantum distribution captured by the ring-polymer Hamiltonian, and it is free of the zero-point energy leaking problem.[50,57] Despite its success on describing

quantum effects in the condensed phase, RPMD is limited to one-electron nonadiabatic dynamics[59–63] or nuclear quantization,[57,64–67] as well as the lack of real-time electronic coherence effects.[59,60] Recently emerged state-dependent RPMD approaches, such as nonadiabatic RPMD (NRPMD),[68–70] mapping variable RPMD (MV-RPMD),[71–73] ring-polymer Ehrenfest dynamics,[74] kinetically constrained RPMD (KC-RPMD),[62,75,76] coherent state RPMD (CS-RPMD),[77] and ring-polymer surface hopping (RPSH),[78–82] are promising to provide accurate nonadiabatic dynamics with an explicit description of electronic states, in addition to the reliable treatment of nuclear quantum effects through the ring polymer quantization.

Among these state-dependent RPMD approaches, NRPMD[68,70] and CS-RPMD[77] have shown to accurately describe both the electronic dynamics and nuclear quantum effects. The NRPMD[68,70] and CS-RPMD[77] Hamiltonian can be viewed as the generalization of the Meyer-Miller-Stock-Thoss (MMST) mapping Hamiltonian[83–85] with the ring-polymer description of the nuclei. Both Hamiltonians have many desired properties, such as a clear adiabatic limit (that returns to the original RPMD Hamiltonian) and one bead limit (that returns to the original MMST Hamiltonian), recovering the correct electronic Rabi oscillations when the electronic states and nuclei are decoupled.[68,70,77] Nevertheless, the promising NRPMD Hamiltonian is *proposed* through a physically motivated but *ad hoc* fashion.[68]

In this paper, we provide a rigorous derivation of the NRPMD Hamiltonian, which is based on the MMST mapping formalism[83–85] for the electronic DOF and the ring polymer path-integral representation[52–54,86] for the nuclear DOF, leading to the same Hamiltonian that has been previously proposed in the NRPMD approach.[68,70] The NRPMD Hamiltonian and the previously derived CS-RPMD Hamiltonian[77] can be viewed as a unified classical theory for electronic states (through the MMST mapping formalism) and nuclei (through the ring polymer quantization).

In addition, we perform numerical simulations to investigate the accuracy of NRPMD Hamiltonian for excited state nonadiabatic dynamics. Despite that RPMD-based approaches are initially developed for investigating quantum dynamics under thermal-equilibrium conditions,[57] recent work based on the Matsubara dynamics framework[87,88] (which does not subject to the restriction of equilibrium conditions[89]) has demonstrated that RPMD yields reliable nonequilibrium time-correlation functions.[89] Furthermore, RPMD-based approaches[59,72,74] have already been used to simulate nonadiabatic dynamics under nonequilibrium initial conditions. These studies inspire us to investigate the performance of NRPMD for simulating excited state nonadiabatic dynamics.

Our numerical results with model calculations suggest that NRPMD can provide an accurate short-time nonadiabatic branching dynamics among many coupled electronic states, as well as the longer time dynamics such as the plateau value of the population or the recurrence of the oscillating electronic population. Quantizing nuclei through a ring polymer instead of using the Wigner distribution alleviates the zero-point energy leakage problem, leading to an accurate electronic quantum dynamics. These encouraging numerical results, together with the rigorous derivation of the NRPMD Hamiltonian, open up new possibilities to accurately simulate nonadiabatic quantum dynamics for an open quantum system.

II. THEORY

In this section, we provide a rigorous derivation of the NRPMD Hamiltonian[68,70] through the imaginary-time path-integral formalism. Furthermore, we propose a numerical procedure to compute the electronic population of the excited state nonadiabatic dynamics. We emphasize that the *dynamics* generated from the NRPMD Hamiltonian in the current work remains a "model dynamics" without a rigorous derivation. Future investigations will focus on the derivation of the NRPMD *dynamics* based on rigorous theoretical frameworks.[69,87,88]

We start by expressing the total Hamiltonian operator as

$$\hat{H} = \hat{T} + \hat{V}_0 + \hat{H}_e = \frac{\hat{\mathbf{P}}^2}{2\mathbf{M}} + V_0(\hat{\mathbf{R}}) + \sum_{n,m=1}^{\mathcal{K}} V_{nm}(\hat{\mathbf{R}})|n\rangle\langle m|, \quad (1)$$

where $\{|n\rangle\}$ is the *diabatic* basis, $\hat{T}$ is the nuclear kinetic energy operator, $\hat{\mathbf{R}} \equiv \{\hat{R}_1, \ldots, \hat{R}_{\mathcal{F}}\}$ is the nuclear position operator associated with $\mathcal{F}$ different nuclear DOFs, with the corresponding conjugate momentum operator $\hat{\mathbf{P}} \equiv \{\hat{P}_1, \ldots, \hat{P}_{\mathcal{F}}\}$ and the nuclear mass $\mathbf{M} \equiv \{M_1, M_2, \ldots, M_{\mathcal{F}}\}$. In addition, $V_0(\hat{\mathbf{R}})$ is the state-independent potential operator, whereas $\hat{H}_e = \sum_{nm} V_{nm}(\hat{\mathbf{R}})|n\rangle\langle m|$ is the state-dependent potential operator (electronic part of the Hamiltonian) with $\mathcal{K}$ total diabatic electronic states.

The canonical partition function of the system is defined as $\mathcal{Z} = \mathrm{Tr}_{\mathrm{en}}[e^{-\beta\hat{H}}]$, where $\mathrm{Tr}_{\mathrm{en}} = \mathrm{Tr}_e\mathrm{Tr}_n$ represents the trace over both the electronic and nuclear DOFs, with $\mathrm{Tr}_e[\ldots] \equiv \sum_{n=1}^{\mathcal{K}}\langle n|\ldots|n\rangle$ and $\mathrm{Tr}_n[\ldots] \equiv \int(\ldots)d\mathbf{R}$. Furthermore, $\beta = 1/k_BT$ is the reciprocal temperature and $\hat{H}$ is the total Hamiltonian operator defined in Eq. (1). The partition function can be exactly evaluated as $\mathcal{Z} = \mathrm{Tr}_{\mathrm{en}}\left[\prod_{\alpha=1}^{N} e^{-\beta_N\hat{H}}\right]$, with a higher effective temperature defined as $\beta_N = \beta/N$. Furthermore, splitting the Boltzmann operator by Trotter expansion under the infinite bead limit $N \to \infty$ gives $\mathcal{Z} = \lim_{N\to\infty}\mathrm{Tr}_{\mathrm{en}}\left[\prod_{\alpha=1}^{N} e^{-\beta_N(\hat{T}+\hat{V}_0)}e^{-\beta_N\hat{H}_e}\right]$. Inserting N copies of the resolution of identity $\hat{I}_{\mathbf{R}} = \int d\mathbf{R}_\alpha|\mathbf{R}_\alpha\rangle\langle\mathbf{R}_\alpha|$ and $\hat{I}_{\mathbf{P}} = \int d\mathbf{P}_\alpha|\mathbf{P}_\alpha\rangle\langle\mathbf{P}_\alpha|$, and explicitly performing the trace over the nuclear DOF based on the standard path-integral technique,[52–54,86] we have

$$\mathcal{Z} = \lim_{N\to\infty}\int d\{\mathbf{P}_\alpha\}d\{\mathbf{R}_\alpha\}e^{-\beta_N H_N^0}\mathrm{Tr}_e\left[\prod_{\alpha=1}^{N} e^{-\beta_N\hat{H}_e(\mathbf{R}_\alpha)}\right], \quad (2)$$

with $\int d\{\mathbf{P}_\alpha\}d\{\mathbf{R}_\alpha\} = \int\prod_{\alpha=1}^{N} d\mathbf{P}_\alpha d\mathbf{R}_\alpha$. The trace over electronic DOF can be performed with diabatic states as $\mathrm{Tr}_e[\ldots] = \sum_{n=1}^{\mathcal{K}}\langle n|\ldots|n\rangle$. The state-independent Hamiltonian H_N^0 is expressed as follows:

$$H_N^0 = \sum_{\alpha=1}^{N}\frac{\mathbf{P}_\alpha^2}{2\mathbf{M}} + \frac{\mathbf{M}}{2\beta_N^2\hbar^2}(\mathbf{R}_\alpha - R_{\alpha-1})^2 + V_0(\mathbf{R}_\alpha), \quad (3)$$

whereas $H_{\mathrm{rp}} = H_N^0 - \sum_\alpha V_0(\mathbf{R}_\alpha)$ is commonly referred to as the free ring-polymer Hamiltonian.[58,90] The above partition function is a common expression for all state-dependent RPMD approaches[68,71,75,91,92] and path-integral Monte-Carlo (PIMC) methods.[93–96] The only difference among these approaches arises from the treatment of the electronic term $\mathrm{Tr}_e[\prod_{\alpha=1}^{N} e^{-\beta_N\hat{H}_e(\mathbf{R}_\alpha)}]$. For example, in the mean-field RPMD approach,[91,92] the electronic

potential is obtained from a weighted average of ring-polymer in different electronic configurations; in the MV-RPMD approach,[71] the electronic states are explicitly described with mapping variables in the Wigner representation; the partition function used in the original NRPMD approach is derived by using mapping variables in both position and momentum bases.[68]

In this work, we adapt the MMST mapping representation[83–85] to transform discrete electronic states into continuous variables. Based on this representation, $\mathcal{K}$ diabatic electronic states are mapped onto $\mathcal{K}$ harmonic oscillators' ground and first excited states through the following relation:

$$|n\rangle \rightarrow |0_1 \dots 1_n \dots 0_{\mathcal{K}}\rangle = \hat{a}_n^\dagger |0_1 \dots 0_n \dots 0_{\mathcal{K}}\rangle. \tag{4}$$

Here, $|0_1 \dots 1_n \dots 0_{\mathcal{K}}\rangle$ is the singly excited oscillator (SEO) state with $(\mathcal{K}-1)$ oscillators in their ground states and the n_{th} oscillator in its first excited state. Thus, the MMST formalism provides[84,85] the following mapping relation:

$$|n\rangle\langle m| \rightarrow \hat{a}_n^\dagger \hat{a}_m, \tag{5}$$

with $\hat{a}_n^\dagger = 1/\sqrt{2\hbar}(\hat{q}_n - i\hat{p}_n)$ and $\hat{a}_m = 1/\sqrt{2\hbar}(\hat{q}_m + i\hat{p}_m)$ as the creation and annihilation operators of the harmonic oscillator, respectively.

With the MMST representation, we express the state-dependent potential operator $\hat{H}_e(\mathbf{R}_\alpha)$ in Eq. (2) as follows:

$$\hat{H}_e(\mathbf{R}_\alpha) \equiv \sum_{n,m} V_{nm}(\mathbf{R}_\alpha)|n\rangle\langle m| \rightarrow \sum_{n,m} V_{nm}(\mathbf{R}_\alpha)\hat{a}_n^\dagger \hat{a}_m. \tag{6}$$

This is commonly referred to as the MMST Hamiltonian.[83,84] Using the above MMST representation, we can derive a partition function that contains the NRPMD Hamiltonian.

A. Derivation of the NRPMD Hamiltonian

We begin by replacing the trace over the electronic DOF in Eq. (2) with the phase space integral of mapping variables in the Wigner representation[69,71,72,97] as follows:

$$\mathrm{Tr_e}\left[\prod_{\alpha=1}^{N} e^{-\beta_N \hat{H}_e(\mathbf{R}_\alpha)}\right] = \frac{1}{(2\pi\hbar)^{\mathcal{K}}} \int d\mathbf{q}_1 d\mathbf{p}_1 \times \left[e^{-\beta_N \hat{H}_e(\mathbf{R}_1)} \prod_{\alpha=2}^{N} e^{-\beta_N \hat{H}_e(\mathbf{R}_\alpha)} \mathcal{P}\right]_{\mathrm{w}_1}. \tag{7}$$

In Eq. (7), the Wigner-Weyl transform[97–99] of the α_{th} bead's mapping DOF is defined as

$$[O]_{\mathrm{w}_\alpha} = \int d\mathbf{\Delta}_\alpha e^{i\mathbf{p}_\alpha^{\mathrm{T}}\mathbf{\Delta}_\alpha/\hbar} \left\langle \mathbf{q}_\alpha - \frac{\mathbf{\Delta}_\alpha}{2} \middle| \hat{\mathrm{O}} \middle| \mathbf{q}_\alpha + \frac{\mathbf{\Delta}_\alpha}{2} \right\rangle. \tag{8}$$

We use the notation $\mathbf{q}_\alpha \equiv \{[\mathbf{q}_\alpha]_1, \dots [\mathbf{q}_\alpha]_n, \dots [\mathbf{q}_\alpha]_{\mathcal{K}}\}$ and $\mathbf{p}_\alpha \equiv \{[\mathbf{p}_\alpha]_1, \dots [\mathbf{p}_\alpha]_n, \dots [\mathbf{p}_\alpha]_{\mathcal{K}}\}$ to represent $\mathcal{K}$ mapping variables for $\mathcal{K}$ electronic states associated with the α_{th} imaginary-time slice. Furthermore, we have inserted an electronic projection operator $\mathcal{P} = \sum_n |n\rangle\langle n|$ to restrain the mapping variables within the SEO subspace.[71,95]

Recall that the Wigner transform has the following property:[97]

$$\int d\mathbf{q}d\mathbf{p}[AB]_{\mathrm{w}} = \int d\mathbf{q}d\mathbf{p}[A]_{\mathrm{w}}[B]_{\mathrm{w}}, \tag{9}$$

where $[AB]_{\mathrm{w}}$, $[A]_{\mathrm{w}}$, and $[B]_{\mathrm{w}}$ are Wigner transforms of operator $\hat{A}\hat{B}$, $\hat{A}$, and $\hat{B}$, respectively, defined in Eq. (8). Using the above equality, we can rewrite Eq. (7) as follows:

$$\begin{aligned}
&\mathrm{Tr_e}\left[\prod_{\alpha=1}^{N} e^{-\beta_N \hat{H}_e(\mathbf{R}_\alpha)}\right] \\
&= \frac{1}{(2\pi\hbar)^{\mathcal{K}}} \int d\mathbf{q}_1 d\mathbf{p}_1 \left[e^{-\beta_N \hat{H}_e(\mathbf{R}_1)} \prod_{\alpha=2}^{N} e^{-\beta_N \hat{H}_e(\mathbf{R}_\alpha)} \mathcal{P}\right]_{\mathrm{w}_1} \\
&= \frac{1}{(2\pi\hbar)^{\mathcal{K}}} \int d\mathbf{q}_1 d\mathbf{p}_1 \left[e^{-\beta_N \hat{H}_e(\mathbf{R}_1)}\right]_{\mathrm{w}_1} \left[\prod_{\alpha=2}^{N} e^{-\beta_N \hat{H}_e(\mathbf{R}_\alpha)} \mathcal{P}\right]_{\mathrm{w}_1} \\
&= \frac{1}{(2\pi\hbar)^{\mathcal{K}}} \int d\mathbf{q}_1 d\mathbf{p}_1 \left[1 - \beta_N \hat{H}_e(\mathbf{R}_1)\right]_{\mathrm{w}_1} \left[\prod_{\alpha=2}^{N} e^{-\beta_N \hat{H}_e(\mathbf{R}_\alpha)} \mathcal{P}\right]_{\mathrm{w}_1} \\
&= \frac{1}{(2\pi\hbar)^{\mathcal{K}}} \int d\mathbf{q}_1 d\mathbf{p}_1 e^{-\beta_N [\hat{H}_e(\mathbf{R}_1)]_{\mathrm{w}_1}} \left[\prod_{\alpha=2}^{N} e^{-\beta_N \hat{H}_e(\mathbf{R}_\alpha)} \mathcal{P}\right]_{\mathrm{w}_1}.
\end{aligned} \tag{10}$$

To derive the last two lines of Eq. (10), we use the fact that under the limit $\beta_N \rightarrow 0$, the Boltzmann operator becomes $e^{-\beta_N \hat{H}_e(\mathbf{R}_1)} = 1 - \beta_N \hat{H}_e(\mathbf{R}_1) + \mathcal{O}(\beta_N^2)$. Under this limit, $[e^{-\beta_N \hat{H}_e(\mathbf{R}_1)}]_{\mathrm{w}_1} = [1 - \beta_N \hat{H}_e(\mathbf{R}_1)]_{\mathrm{w}_1} = 1 - \beta_N [\hat{H}_e(\mathbf{R}_1)]_{\mathrm{w}_1}$. Expressing this term back to the full exponential factor, we arrived at the last line of Eq. (10).

To evaluate $[\hat{H}_e(\mathbf{R}_1)]_{\mathrm{w}_1}$, we use the mapping Hamiltonian relation described in Eq. (6) and the Wigner transform defined in Eq. (8), leading to the following expression:

$$[\hat{H}_e(\mathbf{R}_1)]_{\mathrm{w}_1} = \int d\mathbf{\Delta}_1 e^{i\mathbf{p}_1^{\mathrm{T}}\mathbf{\Delta}_1/\hbar} \left\langle \mathbf{q}_1 - \frac{\mathbf{\Delta}_1}{2} \middle| \sum_{nm} V_{nm}(\mathbf{R}_1)\hat{a}_n^\dagger \hat{a}_m \middle| \mathbf{q}_1 + \frac{\mathbf{\Delta}_1}{2} \right\rangle. \tag{11}$$

To proceed, we use the explicit expressions $\hat{a}_n^\dagger = 1/\sqrt{2\hbar}(\hat{q}_n - i\hat{p}_n)$ and $\hat{a}_m = 1/\sqrt{2\hbar}(\hat{q}_m + i\hat{p}_m)$ and evaluate these Wigner integrals. This derivation is provided in Appendix A, giving the Wigner transformed MMST mapping Hamiltonian of the α_{th} bead as follows:

$$[\hat{H}_e(\mathbf{R}_\alpha)]_{\mathrm{w}_\alpha} = \frac{1}{2\hbar} \sum_{nm} V_{nm}(\mathbf{R}_\alpha) \left([\mathbf{q}_\alpha]_n [\mathbf{q}_\alpha]_m + [\mathbf{p}_\alpha]_n [\mathbf{p}_\alpha]_m - \delta_{nm}\hbar \right). \tag{12}$$

To evaluate $\left[\prod_{\alpha=2}^{N} e^{-\beta_N \hat{H}_e(\mathbf{R}_\alpha)} \mathcal{P}\right]_{\mathrm{w}_1}$ in Eq. (10), we repeat the same procedure used in Eq. (10) for the rest of the imaginary-time slices. The details of this derivation are provided in Appendix A, and here, we briefly summarize the procedure. First, we insert the resolution of identity $\int d\mathbf{q}_2 \mathcal{P}|\mathbf{q}_2\rangle\langle\mathbf{q}_2|$ into $\left[\prod_{\alpha=2}^{N} e^{-\beta_N \hat{H}_e(\mathbf{R}_\alpha)} \mathcal{P}\right]_{\mathrm{w}_1}$. Second, we rearrange the order of terms in the integral and re-express it as a trace over $\mathbf{q}_2$. Finally, replacing the trace over $\mathbf{q}_2$ by a Wigner transform, we can use the property in Eq. (9) again and repeat the same

procedure outlined in Eq. (10) to factorize the total Wigner function as a product of two Wigner functions inside the $\int d\mathbf{q}_2 d\mathbf{p}_2$ integral. Repeating the above outlined process for every single bead, we ended up with the following expression of the electronic trace:

$$\mathrm{Tr_e}\left[\prod_{\alpha=1}^{N} e^{-\beta_N \hat{H}_e(\mathbf{R}_\alpha)}\right] = \frac{1}{(2\pi\hbar)^{N\mathcal{K}}} \int d\{\mathbf{q}_\alpha\} d\{\mathbf{p}_\alpha\} e^{-\beta_N \sum_\alpha [\hat{H}_e(\mathbf{R}_\alpha)]_{w_\alpha}} \times \int d\{\mathbf{\Delta}_\alpha\} \prod_{\alpha=1}^{N} e^{i\mathbf{p}_\alpha^{\mathrm{T}}\mathbf{\Delta}_\alpha/\hbar} \times \left\langle \mathbf{q}_\alpha - \frac{\mathbf{\Delta}_\alpha}{2} | \mathcal{P} | \mathbf{q}_{\alpha+1} + \frac{\mathbf{\Delta}_{\alpha+1}}{2} \right\rangle. \tag{13}$$

Analytically evaluate the last term of Eq. (13)[71] (with details provided in Appendix A), and plugging the result into Eq. (2), we arrive at the final expression of the partition function,

$$\mathcal{Z}_N = \lim_{N\to\infty} \frac{1}{(2\pi\hbar)^{N\mathcal{K}}} \int d\{\mathbf{P}_\alpha\} d\{\mathbf{R}_\alpha\} d\{\mathbf{p}_\alpha\} d\{\mathbf{q}_\alpha\} \mathbf{\Gamma} e^{-\beta_N H_N}, \tag{14}$$

where $\mathbf{\Gamma}$ has the following expression:

$$\mathbf{\Gamma} = \frac{2^{(\mathcal{K}+1)N}}{\hbar^N} \mathrm{Tr_e} \prod_\alpha \left[(\mathbf{q}_\alpha + i\mathbf{p}_\alpha)(\mathbf{q}_\alpha - i\mathbf{p}_\alpha)^{\mathrm{T}} - \frac{\hbar}{2}\mathcal{I} \right] e^{-\frac{1}{\hbar}\sum_\alpha (\mathbf{q}_\alpha^{\mathrm{T}}\mathbf{q}_\alpha + \mathbf{p}_\alpha^{\mathrm{T}}\mathbf{p}_\alpha)}. \tag{15}$$

The derived NRPMD Hamiltonian in Eq. (14), which is one of the *central* results in this paper, has the following expression:

$$H_N = \sum_{\alpha=1}^{N} \left[\frac{\mathbf{P}_\alpha^2}{2M} + V_0(\mathbf{R}_\alpha) + \frac{\mathbf{M}}{2\beta_N^2\hbar^2}(\mathbf{R}_\alpha - \mathbf{R}_{\alpha-1})^2 + \frac{1}{2\hbar}\sum_{nm} V_{nm}(\mathbf{R}_\alpha) \times \left([\mathbf{q}_\alpha]_n [\mathbf{q}_\alpha]_m + [\mathbf{p}_\alpha]_n [\mathbf{p}_\alpha]_m - \delta_{nm}\hbar \right) \right]. \tag{16}$$

The above Hamiltonian has been proposed in the original NRPMD approach,[68,70] and the electronic part of this Hamiltonian [i.e., the second line of Eq. (16)] has also been rigorously derived through a mapping Liouvillian in the state-dependent generalized Kubo-transformed time-correlation function formalism.[69] Here, we provide a rigorous derivation of the full Hamiltonian.

In the NRPMD approach,[68,70] classical trajectories are propagated according to Hamilton's equation of motion associated with H_N in Eq. (16). The motion of the nuclei is governed by $\dot{\mathbf{P}}_\alpha = -\nabla_{\mathbf{R}_\alpha} H_N$ as follows:

$$\dot{\mathbf{P}}_\alpha = -\frac{\mathbf{M}}{\beta_N^2\hbar^2}(2\mathbf{R}_\alpha - \mathbf{R}_{\alpha+1} - \mathbf{R}_{\alpha-1}) - \nabla_{\mathbf{R}_\alpha} V_0(\mathbf{R}_\alpha) - \frac{1}{2\hbar}\sum_{nm} \nabla_{\mathbf{R}_\alpha} V_{nm}(\mathbf{R}_\alpha) \times \left([\mathbf{q}_\alpha]_n [\mathbf{q}_\alpha]_m + [\mathbf{p}_\alpha]_n [\mathbf{p}_\alpha]_m - \delta_{nm}\hbar \right), \tag{17}$$

whereas the bead-specific mapping variables are propagated based on the following Hamilton's equation of motion:

$$[\dot{\mathbf{q}}_\alpha]_n = \frac{\partial H_N}{\partial [\mathbf{p}_\alpha]_n} = \frac{1}{\hbar}\sum_m V_{nm}(\mathbf{R}_\alpha)[\mathbf{p}_\alpha]_m, \qquad [\dot{\mathbf{p}}_\alpha]_n = -\frac{\partial H_N}{\partial [\mathbf{q}_\alpha]_n} = -\frac{1}{\hbar}\sum_m V_{nm}(\mathbf{R}_\alpha)[\mathbf{q}_\alpha]_m. \tag{18}$$

The above NRPMD equations of motion[68,70] have been used to compute approximate Kubo-transformed time-correlation functions under thermal conditions, such as the position autocorrelation function,[68] population autocorrelation function,[68] and absorption spectra[70] based on the Fourier transformed dipole autocorrelation function.

B. Excited states non-adiabatic dynamics with NRPMD

With the derived NRPMD Hamiltonian, we propose to obtain excited state nonadiabatic dynamics by using Hamilton's equation. The central quantity that we aim to compute is the following reduced density matrix for the electronic subsystem:

$$\rho_{jj}(t) = \mathrm{Tr_n}\left[\hat{\rho}_0 e^{i\hat{H}t/\hbar} \hat{\mathcal{P}}_j e^{-i\hat{H}t/\hbar} \right], \tag{19}$$

where $\rho_{jj}(t)$ is the time-dependent population of state $|j\rangle$, $\hat{\mathcal{P}}_j = |j\rangle\langle j|$ is the projection operator associated with state $|j\rangle$, $\mathrm{Tr_n}$ represents the trace over the nuclear DOF, and the initial density operator for the entire system is $\hat{\rho}_0 = |i\rangle\langle i| \otimes \hat{\rho}_\mathrm{n}$, which is a direct product of the initial electronic state projection operator $|i\rangle\langle i|$ and the initial nuclear density operator $\hat{\rho}_\mathrm{n}$.

Despite that the RPMD-based approaches are originally developed for investigating quantum dynamics under thermal-equilibrium conditions,[57] recent work[89] has shown that RPMD yields the exact *nonequilibrium* time-correlation function under high temperatures, short time, and harmonic potential limits through rigorous derivations with the Matsubara dynamics framework,[87,88] which does not subject to any restriction to equilibrium conditions.[89] In that work, RPMD is used to investigate the nonequilibrium (photoinduced) adiabatic dynamics on a single electronic state and has shown to accurately describe quantum dynamics compared to the numerically exact results.[89] Furthermore, the original RPMD method,[59] the MV-RPMD approach,[72] and the state-dependent centroid molecular dynamics approach[100] have already been used to simulate nonadiabatic dynamics under *nonequilibrium* initial conditions. These early studies inspire us to investigate the numerical performance of NRPMD for simulating photoinduced nonequilibrium dynamics.

To compute the time-dependent reduced density matrix $\rho_{jj}(t)$ in Eq. (19), we propose the following expression of population:

$$\rho_{jj}(t) \approx \int d\boldsymbol{\tau} \mathcal{P}^0(\{\mathbf{q}_\alpha(0), \mathbf{p}_\alpha(0)\}) \rho_\mathrm{rp}(\{\mathbf{R}_\alpha(0), \mathbf{P}_\alpha(0)\}) \cdot \bar{\mathcal{P}}_j(t). \tag{20}$$

Here, $d\boldsymbol{\tau} \equiv \int d\{\mathbf{R}_\alpha\} d\{\mathbf{P}_\alpha\} d\{\mathbf{q}_\alpha\} d\{\mathbf{p}_\alpha\}$, with shorthand notation $d\{\boldsymbol{\chi}_\alpha\} = \prod_{\alpha=1}^{N} d\boldsymbol{\chi}_\alpha$. In addition, $\mathcal{P}^0(\{\mathbf{q}_\alpha(0), \mathbf{p}_\alpha(0)\})$ represents the distribution of the initial electronic mapping variables, $\rho_\mathrm{rp}(\{\mathbf{R}_\alpha(0), \mathbf{P}_\alpha(0)\})$ is the ring-polymer density for the initial nuclear density operator $\hat{\rho}_\mathrm{n}$, and $\bar{\mathcal{P}}_j(t)$ is the time-dependent population estimator. The above proposed expression is akin to the excited state population expression used in the MV-RPMD approach.[72]

The electronic population estimator $\bar{\mathcal{P}}$ has many possible choices.[68–70,72] Here, we use the following estimator:

$$\bar{\mathcal{P}}_j = \frac{1}{N}\sum_\alpha \mathcal{P}_j(\alpha) = \frac{1}{N}\sum_{\alpha=1}^{N} \frac{1}{2}([\mathbf{q}_\alpha]_j^2 + [\mathbf{p}_\alpha]_j^2 - 1), \tag{21}$$

which was originally proposed in the NRPMD approach[68] and recently derived in various state-dependent RPMD methods,[69,70] which is also similar to the original MMST population expression.[83,84]

The initial mapping density $\mathcal{P}^0(\mathbf{q}_\alpha(0), \mathbf{p}_\alpha(0))$ is required to describe the initial electronic population $\rho_{jj}(0) = \delta_{ij}$, corresponding to the initially occupied electronic state $|i\rangle$. Here, we adapt the focused initial condition used in the MV-RPMD approach[72,92] and real-time semiclassical path-integral methods[30,101,102] to represent a constrained mapping density,

$$\mathcal{P}^0(\{\mathbf{q}_\alpha(0), \mathbf{p}_\alpha(0)\}) = \prod_{\alpha=1}^{N}\prod_{j=1}^{K}\delta(\mathcal{P}_j(\alpha) - \rho_{jj}(0)). \tag{22}$$

Equation (22) requires the mapping variables to satisfy the following relation:

$$\mathcal{P}_j(\alpha) = \frac{1}{2}([\mathbf{q}_\alpha]_j^2 + [\mathbf{p}_\alpha]_j^2 - 1) = \delta_{ij}. \tag{23}$$

This can be viewed as the "Bohr-Sommerfeld" quantization relation[103] that has been used to initialize mapping variables.[22,38,51,83] Solving Eq. (23) provides the values of the action variables $[\mathbf{q}_\alpha]_j^2 + [\mathbf{p}_\alpha]_j^2$ with a value of 3 for the occupied state $|i\rangle$, and a value of 1 for unoccupied states, whereas the angle variables $[\boldsymbol{\theta}_\alpha]_j = -\tan^{-1}([\mathbf{p}_\alpha]_j/[\mathbf{q}_\alpha]_j)$ are randomly sampled[38,72] within the range of $[0, 2\pi]$. The other choices, such as Window estimators,[38,42,104,105] Wigner transformed projection operators,[106] or MV-RPMD based estimators,[71–73,92] are possible and subject to future investigations.

To compute the nonadiabatic dynamics, real-time trajectories are propagated based on Eqs. (17) and (18), with the mapping and nuclear initial distributions sampled from $\mathcal{P}^0(\{\mathbf{q}_\alpha(0), \mathbf{p}_\alpha(0)\})$ and $\rho_{\mathrm{rp}}(\{\mathbf{R}_\alpha(0), \mathbf{P}_\alpha(0)\})$, respectively. The time-dependent population is computed based on the ensemble average described in Eq. (20).

C. Computational details

1. Model systems

In this paper, we adapt two widely used model systems to investigate the performance of NRPMD for simulating excited state nonadiabatic dynamics. Both models contain several electronic states coupled to a nuclear vibrational mode. Despite only containing one nuclear mode, the electronic subsystem is indeed an open quantum system due to the interaction with its environment (i.e., the nuclear DOF). This interaction causes nonunitary quantum dynamics for the electronic subsystem, whereas the composite electronic-nuclear system exhibits unitary quantum dynamics.[3]

Model I is a widely used three-state Morse potential for photodissociation dynamics.[107] The Hamiltonian operator $\hat{H} = \hat{P}^2/2M + \hat{V}$ of model I has the following potential:

$$\begin{aligned} V_{ii} &= \langle i|\hat{V}|i\rangle = D_{ii}(1 - e^{-\alpha_{ii}(R-R_{ii})})^2 + c_{ii}, \\ V_{ij} &= \langle i|\hat{V}|j\rangle = A_{ij}e^{-\alpha_{ij}(R-R_{ij})^2}. \end{aligned} \tag{24}$$

Here, V_{ii} and V_{ij} are diabatic potentials and couplings, respectively. Parameters of model I are provided in Table I. These potentials and couplings are visualized in Figs. 1(a)–1(c). The nuclear mass is $M = 20\,000$ a.u.

Model II is a one dimensional spin-boson system[68,71,108] with the following Hamiltonian:

$$\hat{H} = \frac{\hat{P}^2}{2M} + \frac{1}{2}M\omega^2\hat{R}^2 + \sqrt{2}\gamma\hat{\sigma}_z \otimes \hat{R} + \frac{\Delta}{2}\hat{\sigma}_x. \tag{25}$$

In Eq. (23), $\hat{\sigma}_z$ and $\hat{\sigma}_x$ are Pauli spin matrices in the electronic subspace $\{|1\rangle, |2\rangle\}$, $\Delta = 1$ a.u., $\hat{R}$ and $\hat{P}$ are the position and momentum operators of a harmonic boson mode with frequency $\omega = 1$ a.u., respectively, and the nuclear mass is $M = 1$ a.u. The two-level system and the boson mode interact with each other through a bilinear coupling potential with a constant coupling strength γ.

2. Initial conditions

For all results presented in this work, the initial photoexcitation is modeled by the following density operator:

$$\hat{\rho} = |1\rangle\langle 1| \otimes \hat{\rho}_{\mathrm{n}}, \tag{26}$$

where $|1\rangle$ is the first diabatic state in both models and the initial nuclear density operator is

TABLE I. Parameters for model IA-IC (in atomic units).

	Model IA			Model IB			Model IC		
i	1	2	3	1	2	3	1	2	3
D_{ii}	0.02	0.02	0.003	0.02	0.01	0.003	0.003	0.004	0.003
α_{ii}	0.4	0.65	0.65	0.65	0.4	0.65	0.65	0.6	0.65
R_{ii}	4.0	4.5	6.0	4.5	4.0	4.4	5.0	4.0	6.0
c_{ii}	0.02	0.0	0.02	0.0	0.01	0.02	0.0	0.01	0.006
ij	12	13	23	12	13	23	12	13	23
A_{ij}	0.005	0.005	0.0	0.005	0.005	0.0	0.002	0.0	0.002
α_{ij}	32.0	32.0	0.0	32.0	32.0	0.0	16.0	0.0	16.0
R_{ij}	3.40	4.97	0.0	3.66	3.34	0.0	3.40	0.0	4.8

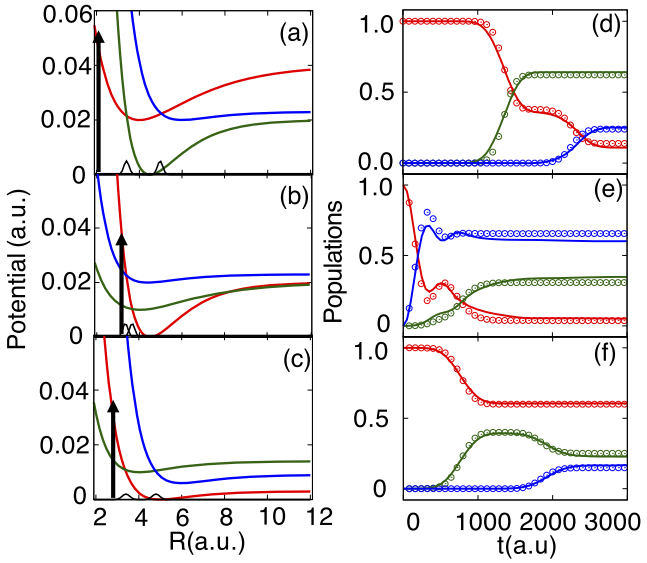

FIG. 1. (a)–(c) present diabatic potentials for models IA-IC, with diabatic state $|1\rangle$ (red), $|2\rangle$ (green), and $|3\rangle$ (blue). The diabatic couplings are indicated with black solid lines, and the initial Franck-Condon excitation is illustrated with black arrows. The ground electronic state is not shown. (d)–(f) present the real-time population dynamics obtained from the NRPMD propagation (open circles) and numerically exact results (solid lines). The populations are color-coded corresponding to the diabatic surfaces.

$$\hat{\rho}_{\rm n} = e^{-\beta \hat{H}_{\rm g}(\hat{R},\hat{P})}. \tag{27}$$

The above initial nuclear density is chosen as the canonical thermal density associated with the ground state Hamiltonian,

$$\hat{H}_{\rm g} = \frac{\hat{P}^2}{2M} + \frac{1}{2}M\omega_0^2(\hat{R} - R_0)^2, \tag{28}$$

where M is the nuclear mass and R_0 is the position of the Franck-Condon vertical excitation. Here, we assume that the ground state and the excited states are electronically decoupled; there is no communication between them except during the initial photoexcitation. For model I, the initial excitation is indicated with black arrows in Figs. 1(a)–1(c), with R_0 = 2.1, 3.3, and 2.9 for models IA, IB, and IC, respectively. The frequency of the ground state is chosen[72] as ω_0 = 0.005 a.u., and β is the inverse temperature that corresponds to 300 K. For model II, R_0 = 0, the frequency of the ground state is ω_0 = 1 a.u., and the inverse temperature is chosen as β = 16 a.u. such that the initial nuclear quantum distribution is significantly different compared to the classical one, and the dynamics cannot be accurately treated through the classical Wigner model (that samples the initial Wigner distribution and propagates the trajectories classically).

3. Simulation details

For all NRPMD results presented in this paper, a total of 10^4 trajectories are used to generate the converged population dynamics. Each configuration is then propagated by using Eqs. (17) and (18). A symplectic integration scheme is used to numerically propagate the dynamics,[109,110] although the other simpler scheme[70] generates the same numerical results for the model calculations studied here. The initial conditions for the mapping variables are sampled based on Eq. (23).

The initial thermal nuclear density $\hat{\rho}_n$ is sampled by the normal-mode path-integral Monte-Carlo (PIMC)[111] in the ground state $\hat{H}_{\rm g}$ [Eq. (28)], which generates the ring-polymer initial density,

$$\rho_{\rm rp}(\mathbf{R}_\alpha, \mathbf{P}_\alpha) = e^{-\beta_N H_N^{\rm g}(\mathbf{R}_\alpha, \mathbf{P}_\alpha)}. \tag{29}$$

In Eq. (29), $\beta_N = \beta/N$, with N being the number of beads (imaginary-time slices), and the ring-polymer Hamiltonian associated with the ground state $\hat{H}_{\rm g}$ is expressed as follows:

$$H_N^{\rm g} = \sum_{\alpha=1}^{N} \frac{P_\alpha^2}{2M} + \frac{M}{2\beta_N^2\hbar^2}(R_\alpha - R_{\alpha+1})^2 + \frac{1}{2}M\omega_0^2(R_\alpha - R_0)^2. \tag{30}$$

In this study, we follow the recent works of state-dependent RPMD that treat N as a convergence parameter.[70,72] For the sampling of the nuclear initial condition [Eq. (29)], a large enough N is used to ensure a converged $\rho_{\rm rp}(\mathbf{R}_\alpha, \mathbf{P}_\alpha)$. This requires N = 4 for model I and N = 16 for model II, and N remains fixed for the dynamics propagation. We have also performed convergence tests for population dynamics with a higher number of beads, suggesting that these choices of N are sufficient to provide converged results. A specific example of the bead convergence is provided in Appendix A.

The real-time NRPMD dynamics governed by H_N [Eq. (16)] requires a fictitious temperature β^{-1} as the parameter of the dynamics.[72,79,112] For model I, we follow the previous MV-RPMD work[72] on choosing β^{-1}, which corresponds to the zero-point energy (ZPE) of the ground state plus the potential energy gap between the lowest excited state and the initially occupied excited state at R_0. This provides the fictitious temperatures of 15 288 K, 9605 K, and 8843 K for models IA, IB, and IC, respectively.[72] For model II, we directly use β = 16 (associated with the initial distribution) during the NRPMD simulation.

Numerically exact results for model I are obtained from the discrete variable representation (DVR) calculations,[113] with a grid spacing of 0.009 a.u. in the range of $R \in$ [0.5, 20] a.u. For model II, exact results are directly obtained by computing the reduced density matrix $\rho_{jj}(t) = {\rm Tr}_{\rm n}[\hat{\rho}_0 e^{i\hat{H}t/\hbar}|j\rangle\langle j|e^{-i\hat{H}t/\hbar}]$ evaluated with the basis $|i\rangle \otimes |n\rangle$, where $|i\rangle$ is the diabatic basis in model II and $|n\rangle$ is the eigenstate of the harmonic oscillator centered at R = 0.

III. RESULTS AND DISCUSSION

Figure 1 presents the population dynamics of models IA-IC for photoinduced dissociation dynamics. (a)–(c) present the diabatic potentials. Black arrows indicate the Franck-Condon vertical excitations. (d)–(f) provide the diabatic populations with the same color coding used in (a)–(c) for the diabatic states, obtained from NRPMD simulations (open circles) as well as numerically exact results (solid lines). For all three cases, NRPMD provides a reasonable agreement with the exact results for both the short-time relaxation and nonadiabatic branching dynamics, as well as the longer time asymptotic populations. We emphasize that model I is a challenging test case for many approximate nonadiabatic dynamics approaches[39,72,107,114] due to its highly anharmonic potential and nonlinear diabatic couplings. Nevertheless, NRPMD provides accurate predictions for the key features of these nonadiabatic events associated with multiple curve crossings.

Figure 2 presents the state-dependent population dynamics of model IA computed from various recently developed methods, including (a) NRPMD [same as in Fig. 1(d)], (b) partial linearized density matrix (PLDM) path-integral approach,[32,114] (c) MV-RPMD approach,[71,72] and (d) symmetrical quasiclassical (SQC) approach.[39,103,105] Here, we are interested in comparing the nonadiabatic dynamics generated from different forms of the Hamiltonian. All of these trajectory-based approaches converge with approximately 10^4 trajectories. The RPMD-based approaches require an extended phase-space description for all DOF, thus further increasing the numerical cost. In (b), PLDM generates accurate short-time nonadiabatic branching dynamics but starts to deviate from the exact result later, potentially due to the less accurate partial linearization approximation at a longer time.[32,114] This can be fixed by using an *iterative* version of PLDM,[33,115] which only requires the linearization approximation at short times and then concatenates these short-time PLDM propagators through a Monte Carlo sampling procedure.[33,102,115] The iterative-PLDM provides accurate dynamics for model I, although a large number of trajectories (10^6) are required to converge the result.[115] Furthermore, the PLDM Hamiltonian can be viewed as a particular limit of the NRPMD Hamiltonian (or the CS-RPMD Hamiltonian[77]) with one nuclear bead and two mapping beads (for describing the forward and backward propagations).[32] NRPMD which uses multiple beads for all DOFs seems to provide more accurate short-time branching dynamics as well as long-time populations.

In Fig. 2(c), the MV-RPMD approach[72] provides less accurate nonadiabatic branching dynamics, probably due to the presence of the interbead coupling of the mapping variables, which contaminates the electronic dynamics.[68,71] Furthermore, its inability to correctly capture electronic coherence[116] could also mitigate its accuracy of describing the quantum branching dynamics. The NRPMD Hamiltonian, on the other hand, does not contain any interbead coupling for mapping variables and thus can reliably capture electronic coherence dynamics[68,70] and provide accurate nonadiabatic population transfer as shown in Fig. 2(a).

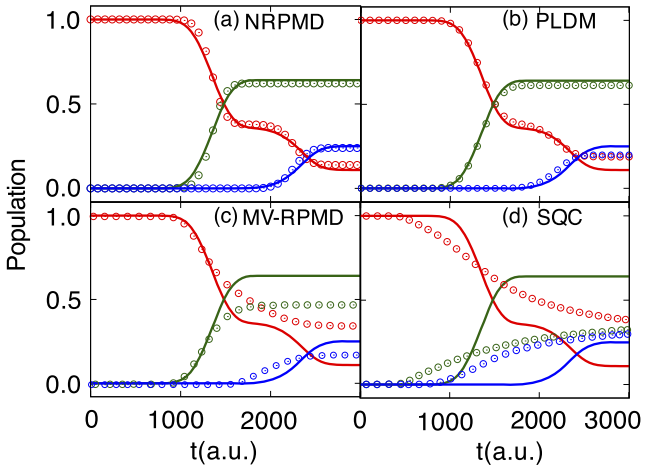

FIG. 2. Population dynamics of model IA obtained from (a) NRPMD, (b) partial linearized density matrix (PLDM) path-integral approach,[114] (c) MV-RPMD,[72] and (d) symmetrical quasiclassical (SQC) approach.[39] The results from these approximate trajectory-based approaches are represented by circles, whereas the numerically exact results are depicted with solid lines.

In Fig. 2(d), the recently developed SQC[38,39,105] approach provides less accurate results for this model compared to the other three approaches. Despite that SQC provides accurate nonadiabatic dynamics for many model systems,[38] the population dynamics for model IA starts to deviate from the exact results even at a very short time. This is also the case for models IB and IC.[39] Furthermore, the closely related Linearized Semiclassical Initial Value Representation (LSC-IVR) approach generates very similar results compared to SQC, except some negative populations.[72,107,114] These results suggest that the Ehrenfest type of the nuclear force, together with the nuclear Wigner distribution (used by both SQC and LSC-IVR), could be the cause for this less accurate dynamics. A recently proposed coherence-controlled SQC (cc-SQC) approach[39] has significantly improved the results by using different nuclear forces based on the time-dependent action variables.[39]

Figure 3 presents the population difference $\langle\sigma_z(t)\rangle$ between state $|1\rangle$ and $|2\rangle$ in model II with three different electron-phonon coupling strengths γ/Δ. Here, we compare the dynamics obtained from NRPMD (red) with multitrajectory Ehrenfest (MTEF) dynamics (green), PLDM (blue), and numerically exact simulations (black). (a) presents the results in a weak electron-phonon coupling regime with $\gamma/\Delta = 0.1$. The temperature $\beta = 16$ is low enough such that the initial quantum distribution is significantly different compared to the classical distribution. Thus, a quantum mechanical treatment of the nuclear DOF is required for trajectory-based approaches, through the Wigner initial distribution (for MTEF and PLDM) or the ring polymer quantization (for NRPMD). One can see that all three approximate methods behave accurately compared to the numerically exact results and reproduce correct oscillations and damping patterns up to $t = 15$ a.u. After that, both the PLDM and MTEF approach fail[108] to accurately describe the longer time recurrence of oscillation in $\langle\sigma_z(t)\rangle$. This less accurate longer time dynamics might be caused by the zero point energy (ZPE) leakage,[50,117] which is typical for linearized path-integral approaches based on the classical Wigner dynamics.[22,29,118] This ZPE leakage originates from the fact that classical dynamics does not preserve the ZPE incorporated in the initial Wigner distribution,[50,117] causing an incorrect energy flow from the nuclear DOF to the electronic DOF[51] and equalizing the longer time populations. Compared to the classical Wigner treatment of the nuclear DOF,[22,29,118] quantizing the nuclear DOF with the ring polymer can effectively incorporate nuclear ZPE through an extended phase-space description[78–81] and alleviate ZPE leakage, thus accurately providing the longer time recurrence of the oscillating electronic population.

Figures 3(b) and 3(c) present the population dynamics for model II with stronger electron-phonon couplings. We can see that the NRPMD method reproduces the exact result fairly well up to $t = 5$ a.u. At a longer time, however, NRPMD becomes less accurate compared to the exact results, missing the recurrence of the oscillations. These deviations at a longer time in (b) and (c) might be due to the intrinsic quantum coherence of nuclear dynamics, which is missed by NRPMD while can be captured by methods that employ coupled trajectories.[108] Nevertheless, as an independent trajectory-based approach, NRPMD still outperforms both MTEF and PLDM for all model calculations presented here.

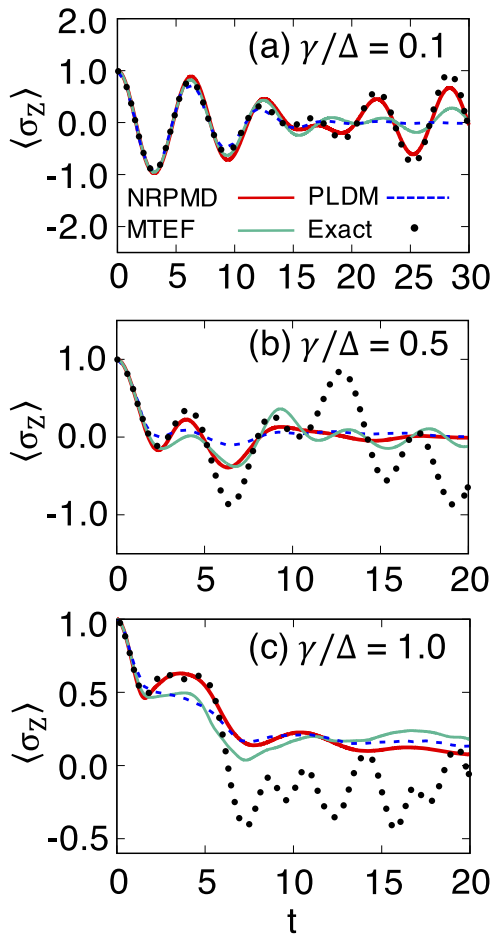

FIG. 3. Population dynamics $\langle\sigma_z(t)\rangle$ of model II with various electron-photon couplings at (a) $\gamma/\Delta = 0.1$, (b) $\gamma/\Delta = 0.5$, and (c) $\gamma/\Delta = 1.0$. Results are obtained from NRPMD (red solid line), multitrajectory Ehrenfest (MTEF) dynamics depicted with the green solid line, PLDM depicted with blue dashed lines, and numerically exact results with black dots.

We emphasize that the success of any RPMD-based approach relies on the separation of the time scale between the high-frequency vibrations of the ring polymer and the dynamics of physical interest.[57] The high-frequency ring polymer oscillations could contaminate the real-time dynamics of the nuclei, which in turn influence the electronic quantum dynamics. This issue could potentially impact the accuracy of our population dynamics, for example, slightly shifting the electronic Rabi oscillation of $\langle\sigma_z(t)\rangle$ in Fig. 3. To address it, we incorporate the recently developed thermostatting technique[90,119,120] to NRPMD, with details provided in Appendix B. Thermostatting has been shown to successfully remove these contaminations from spurious high-frequency oscillations,[120] and the model calculations provided in Appendix B confirm that correct electronic Rabi frequency is recovered when applying a Langevin thermostat on the nuclear ring polymer normal modes. Thus, thermostatting offers a valuable and practical approach to remove contaminations from the high-frequency ring polymer vibrations, enables the promising NRPMD approach to provide more accurate excited state nonadiabatic dynamics.

IV. CONCLUSION

In this paper, we present a rigorous derivation of the NRPMD Hamiltonian that was originally proposed.[68] Our derivation uses the MMST mapping representation for the electronic DOF and the ring polymer path-integral quantization for the nuclear DOF. The NRPMD Hamiltonian, together with the previously derived CS-RPMD Hamiltonian,[77] can be viewed as a unified theory for classical electronic states (through the MMST mapping description) and classical nuclei (through the ring polymer quantization).

We further propose a procedure to compute excited state nonadiabatic quantum dynamics[72,89] with the NRPMD Hamiltonian. Numerical results with the coupled Morse potential and one-dimensional spin-boson model suggest that NRPMD can provide accurate short-time branching dynamics and a reliable longer time dynamics. The NRPMD Hamiltonian does not contain interbead coupling terms associated with the electronic mapping variables; thus, it is capable of accurately capturing the electronic quantum dynamics.[68,70] In a particular coupled Morse potential model system, NRPMD outperforms the recently developed MV-RPMD methods[71,72] which do include these interbead coupling terms that might contaminate the electronic dynamics. Compared to the linearized semiclassical methods based on the Wigner quantization of nuclei,[22,29,32] quantizing the nuclear DOF with ring polymer can effectively incorporate nuclear zero-point energy (ZPE) and alleviates the ZPE leakage problem.

This work opens up new possibilities of using state-dependent RPMD approaches[68,70,77] to accurately simulate nonadiabatic dynamics for electronic open quantum systems. These approaches are also potentially well-suited theoretical methods to investigate photochemical reactions, especially when nuclear quantum effects play an important role, such as in the photoinduced proton-coupled electron transfer reactions.[121–127] We note that the original RPMD method is limited to one electron nonadiabatic process,[57,59–63] whereas the vibronic quantization approach (which uses an explicit quantum-state description of proton) can be numerically expensive for a three-dimensional quantum treatment of many protons.[122,123,125–129] State-dependent RPMD approaches, such as NRPMD[68] and CS-RPMD,[77] provide accurate electronic nonadiabatic dynamics and nuclear quantum effects without any limitations on the number of electrons and protons that can be explicitly described.

Most of the state-dependent RPMD approaches, including the NRPMD method discussed here, are formulated in the *diabatic* representation. To perform on-the-fly simulation with adiabatic electronic structure calculations, these approaches are usually reformulated back to the adiabatic representation. This process requires nontrivial theoretical efforts, and the adiabatic equation of motion is computationally inconvenient due to the presence of derivative couplings. These nontrivial tasks, however, can be avoided by using the recently developed quasidiabatic propagation scheme.[130] The quasidiabatic (QD) scheme uses the adiabatic states associated with a reference geometry as the local diabatic states during a short-time propagation step and dynamically updates the definition of the diabatic states along the time-dependent nuclear trajectory. This scheme thus allows a seamless interface between diabatic dynamics approaches (such as NRPMD) with adiabatic electronic structure calculations, providing new frameworks

to accurately and efficiently perform nonadiabatic on-the-fly simulations.

Future investigations will also focus on analytic derivation of the NRPMD *dynamics* based on rigorous theoretical frameworks,[87,88,131,132] such as the Matsubara dynamics[87,88] and the exact mapping Liouvillian.[69] These formal theoretical derivations will help to assess the validity and the accuracy of the state-dependent RPMD approaches for simulating excited state nonadiabatic dynamics.

ACKNOWLEDGMENTS

This work was supported by the National Science Foundation CAREER Award under Grant No. CHE-1845747. Computing resources were provided by the Center for Integrated Research Computing (CIRC) at the University of Rochester.

APPENDIX A: DETAILS OF THE DERIVATION FOR NRPMD PARTITION FUNCTION

In this appendix, we provide details of the derivations for (i) the expression of $[\hat{H}_e(\mathbf{R}_\alpha)]_{w_\alpha}$ in Eq. (12), (ii) the expression of the electronic partition function $\mathrm{Tr}_e[\prod_{\alpha=1}^{N} e^{-\beta_N \hat{H}_e(\mathbf{R}_\alpha)}]$ in Eq. (13), and (iii) the expression of $\mathbf{\Gamma}$ in Eq. (15).

First, we provide the derivation of the $[\hat{H}_e(\mathbf{R}_\alpha)]_{w_\alpha}$ expression. The Wigner transformed mapping Hamiltonian operator [Eq. (6)] can be expressed as follows:

$$
\begin{aligned}
[\hat{H}_e(\mathbf{R}_\alpha)]_{w_\alpha} &= \int d\mathbf{\Delta}_\alpha e^{i\mathbf{p}_\alpha^T\mathbf{\Delta}_\alpha/\hbar}\left\langle \mathbf{q}_\alpha - \frac{\mathbf{\Delta}_\alpha}{2}\middle|\sum_{nm} V_{nm}(\mathbf{R}_\alpha)\frac{1}{2\hbar}\left(\hat{q}_n\hat{q}_m + \hat{p}_n\hat{p}_m - \delta_{nm}\hbar\right)\middle|\mathbf{q}_\alpha + \frac{\mathbf{\Delta}_\alpha}{2}\right\rangle \\
&= \frac{1}{2\hbar}\sum_{nm} V_{nm}(\mathbf{R}_\alpha)\int d\mathbf{\Delta}_\alpha e^{i\mathbf{p}_\alpha^T\mathbf{\Delta}_\alpha/\hbar}\left[\left(\mathbf{q}_\alpha - \frac{\mathbf{\Delta}_\alpha}{2}\right)_n\left(\mathbf{q}_\alpha + \frac{\mathbf{\Delta}_\alpha}{2}\right)_m - \hbar^2\frac{\partial}{\partial[\mathbf{\Delta}_\alpha]_n}\frac{\partial}{\partial[\mathbf{\Delta}_\alpha]_m} - \delta_{nm}\hbar\right]\delta(\mathbf{\Delta}_\alpha) \\
&= \frac{1}{2\hbar}\sum_{nm} V_{nm}(\mathbf{R}_\alpha)\left[[\mathbf{q}_\alpha]_n[\mathbf{q}_\alpha]_m - \hbar^2\int d\mathbf{\Delta}_\alpha\delta(\mathbf{\Delta}_\alpha)\frac{\partial}{\partial[\mathbf{\Delta}_\alpha]_n}\frac{\partial}{\partial[\mathbf{\Delta}_\alpha]_m}e^{i\mathbf{p}_\alpha^T\mathbf{\Delta}_\alpha/\hbar} - \delta_{nm}\hbar\int d\mathbf{\Delta}_\alpha\delta(\mathbf{\Delta}_\alpha)e^{i\mathbf{p}_\alpha^T\mathbf{\Delta}_\alpha}\right] \\
&= \frac{1}{2\hbar}\sum_{nm} V_{nm}(\mathbf{R}_\alpha)\left([\mathbf{q}_\alpha]_n[\mathbf{q}_\alpha]_m + [\mathbf{p}_\alpha]_n[\mathbf{p}_\alpha]_m - \delta_{nm}\hbar\right).
\end{aligned}
\tag{A1}
$$

Between the first and the second equality, we have used the fact $\langle q - \frac{\Delta}{2}|\hat{p}|q + \frac{\Delta}{2}\rangle = \int dpp\langle q - \frac{\Delta}{2}|p\rangle\langle p|q + \frac{\Delta}{2}\rangle = (\frac{1}{2\pi\hbar})\int dppe^{-\frac{i}{\hbar}p\Delta} = (\frac{1}{2\pi\hbar})i\hbar\frac{\partial}{\partial\Delta}\int dpe^{-\frac{i}{\hbar}p\Delta} = i\hbar\frac{\partial}{\partial\Delta}\int dp\langle q - \frac{\Delta}{2}|p\rangle\langle p|q + \frac{\Delta}{2}\rangle = i\hbar\frac{\partial}{\partial\Delta}\langle q - \frac{\Delta}{2}|q + \frac{\Delta}{2}\rangle$. Between the second and the third equality, we use integration by parts for $\int d\mathbf{\Delta}_\alpha$. Analytically perform the rest integrals, we arrived at the final expression of $[\hat{H}_e(\mathbf{R}_\alpha)]_{w_\alpha}$ in Eq. (12). The same derivation has also been used in the Wigner mapping mixed quantum-classical Liouville (MQCL) equation.[133]

Second, we provide the details of the derivation for the electronic trace expression in Eq. (13). We start by inserting a resolution of identity $\int d\mathbf{q}_2\mathcal{P}|\mathbf{q}_2\rangle\langle\mathbf{q}_2|$ into $\left[\prod_{\alpha=2}^{N} e^{-\beta_N\hat{H}_e(\mathbf{R}_\alpha)}\mathcal{P}\right]_{w_1}$, resulting in the second line of Eq. (A2). Next, we alter the order of terms in lines 3 and 4 of Eq. (A2), leading to an integral over $\mathbf{q}_2$. Finally, replacing $\int d\mathbf{q}_2$ by the corresponding Wigner transform,[72] we can use the property in Eq. (9) again and repeat the same procedure outlined in Eq. (10) to factorize the total Wigner function as a product of two Wigner functions inside the $\int d\mathbf{q}_2 d\mathbf{p}_2$ integral, arriving at the last line of the following equation:

$$
\begin{aligned}
\mathrm{Tr}_e\left[\prod_{\alpha=1}^{N} e^{-\beta_N\hat{H}_e(\mathbf{R}_\alpha)}\right] &= \frac{1}{(2\pi\hbar)^{\mathcal{K}}}\int d\mathbf{q}_1 d\mathbf{p}_1 e^{-\beta_N[\hat{H}_e(\mathbf{R}_1)]_{w_1}}\left[\int d\mathbf{q}_2\mathcal{P}|\mathbf{q}_2\rangle\langle\mathbf{q}_2|\prod_{\alpha=2}^{N} e^{-\beta_N\hat{H}_e(\mathbf{R}_\alpha)}\mathcal{P}\right]_{w_1} \\
&= \frac{1}{(2\pi\hbar)^{\mathcal{K}}}\int d\mathbf{q}_1 d\mathbf{p}_1 e^{-\beta_N[\hat{H}_e(\mathbf{R}_1)]_{w_1}}\int d\mathbf{\Delta}_1 e^{i\mathbf{p}^T\mathbf{\Delta}_1/\hbar}\left\langle\mathbf{q}_1 - \frac{\mathbf{\Delta}_1}{2}\middle|\int d\mathbf{q}_2\mathcal{P}|\mathbf{q}_2\rangle\langle\mathbf{q}_2|\prod_{\alpha=2}^{N} e^{-\beta_N\hat{H}_e(\mathbf{R}_\alpha)}\mathcal{P}\middle|\mathbf{q}_1 + \frac{\mathbf{\Delta}_1}{2}\right\rangle \\
&= \frac{1}{(2\pi\hbar)^{\mathcal{K}}}\int d\mathbf{q}_1 d\mathbf{p}_1 e^{-\beta_N[\hat{H}_e(\mathbf{R}_1)]_{w_1}}\int d\mathbf{\Delta}_1 e^{i\mathbf{p}^T\mathbf{\Delta}_1/\hbar}\int d\mathbf{q}_2\left\langle\mathbf{q}_2\middle|e^{-\beta_N\hat{H}_e(\mathbf{R}_2)}\prod_{\alpha=3}^{N} e^{-\beta_N\hat{H}_e(\mathbf{R}_\alpha)}\mathcal{P}\middle|\mathbf{q}_1 + \frac{\mathbf{\Delta}_1}{2}\right\rangle\left\langle\mathbf{q}_1 - \frac{\mathbf{\Delta}_1}{2}\middle|\mathcal{P}\middle|\mathbf{q}_2\right\rangle \\
&= \frac{1}{(2\pi\hbar)^{2\mathcal{K}}}\int d\mathbf{q}_1 d\mathbf{p}_1 e^{-\beta_N[\hat{H}_e(\mathbf{R}_1)]_{w_1}}\int d\mathbf{\Delta}_1 e^{i\mathbf{p}_1^T\mathbf{\Delta}_1/\hbar}\int d\mathbf{q}_2 d\mathbf{p}_2\left[e^{-\beta_N\hat{H}_e(\mathbf{R}_2)}\prod_{\alpha=3}^{N} e^{-\beta_N\hat{H}_e(\mathbf{R}_\alpha)}\mathcal{P}|\mathbf{q}_1 + \frac{\mathbf{\Delta}_1}{2}\rangle\langle\mathbf{q}_1 - \frac{\mathbf{\Delta}_1}{2}|\mathcal{P}\right]_{w_2} \\
&= \frac{1}{(2\pi\hbar)^{2\mathcal{K}}}\int d\mathbf{q}_1 d\mathbf{p}_1 e^{-\beta_N[\hat{H}_e(\mathbf{R}_1)]_{w_1}}\int d\mathbf{\Delta}_1 e^{i\mathbf{p}_1^T\mathbf{\Delta}_1/\hbar}\int d\mathbf{q}_2 d\mathbf{p}_2 e^{-\beta_N[\hat{H}_e(\mathbf{R}_2)]_{w_2}}\left[\prod_{\alpha=3}^{N} e^{-\beta_N\hat{H}_e(\mathbf{R}_\alpha)}\mathcal{P}|\mathbf{q}_1 + \frac{\mathbf{\Delta}_1}{2}\rangle\langle\mathbf{q}_1 - \frac{\mathbf{\Delta}_1}{2}|\mathcal{P}\right]_{w_2}.
\end{aligned}
\tag{A2}
$$

A similar procedure of the above derivation has been recently used to derive the population estimator in the MV-RPMD approach.[72]

Third, we derive the expression of $\mathbf{\Gamma}$ [Eq. (15)]. We start from the last line of Eq. (13) and define

$$\mathbf{\Gamma} = \prod_{\alpha=1}^{N} \int d\mathbf{\Delta}_\alpha e^{i\mathbf{p}_\alpha^{\mathrm{T}}\mathbf{\Delta}_\alpha/\hbar} \left\langle \mathbf{q}_\alpha - \frac{\mathbf{\Delta}_\alpha}{2} | \mathcal{P} | \mathbf{q}_{\alpha+1} + \frac{\mathbf{\Delta}_{\alpha+1}}{2} \right\rangle, \tag{A3}$$

where $\mathcal{P} = \sum_n |n\rangle\langle n|$ is the projection operator in the SEO basis. Recall that the SEO mapping wavefunction is the product of $(\mathcal{K}-1)$ ground state harmonic oscillator wavefunctions and one excited state harmonic oscillator wavefunction,

$$\langle \mathbf{q}|n\rangle = \sqrt{\frac{2}{\hbar}} \frac{1}{(\pi\hbar)^{\mathcal{K}/4}} [\mathbf{q}]_n e^{-\mathbf{q}^{\mathrm{T}}\mathbf{q}/2\hbar}. \tag{A4}$$

With Eq. (A4), we can rewrite Eq. (A3) as

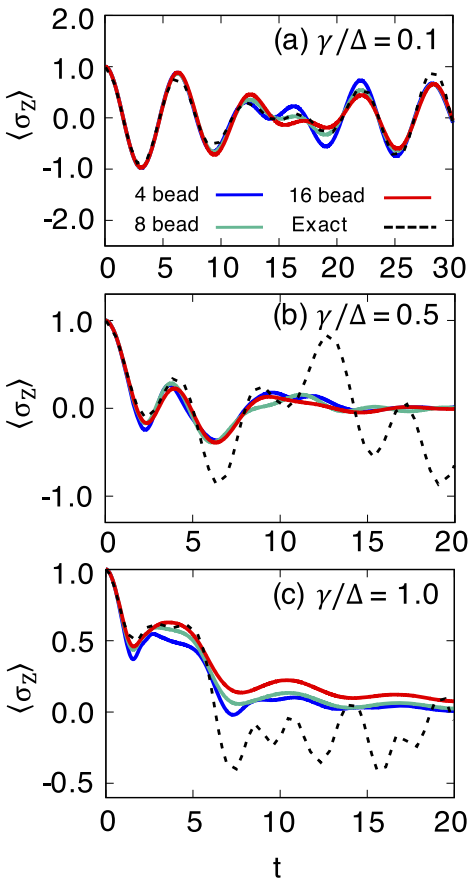

FIG. 4. Bead convergence of the population dynamics for model II with various electron-photon couplings at (a) $\gamma/\Delta = 0.1$, (b) $\gamma/\Delta = 0.5$, and (c) $\gamma/\Delta = 1.0$. The blue, green, and red lines show the results obtained from 4, 8, and 16 bead NRPMD simulations, respectively. Numerically exact results are depicted with black dashed lines. The results converge with 16 beads compared to the 32 bead results (not shown).

$$\mathbf{\Gamma} = \frac{2^N}{\hbar^N} \frac{1}{(\pi\hbar)^{N\mathcal{K}/2}} \prod_{\alpha=1}^{N} \int d\mathbf{\Delta}_\alpha \left(\mathbf{q}_\alpha - \frac{\mathbf{\Delta}_\alpha}{2}\right)^{\mathrm{T}} \left(\mathbf{q}_{\alpha+1} + \frac{\mathbf{\Delta}_{\alpha+1}}{2}\right) \times e^{-\frac{1}{\hbar}\left(\frac{1}{4}\mathbf{\Delta}_\alpha^{\mathrm{T}}\mathbf{\Delta}_\alpha + \mathbf{q}_\alpha^{\mathrm{T}}\mathbf{q}_\alpha - i\mathbf{p}_\alpha^{\mathrm{T}}\mathbf{\Delta}_\alpha\right)}. \tag{A5}$$

Rearranging the prefactors of Eq. (A5) and grouping terms associated with $\mathbf{\Delta}_\alpha$, we have

$$\mathbf{\Gamma} = \frac{2^N}{\hbar^N} \frac{1}{(\pi\hbar)^{N\mathcal{K}/2}} \int d\{\mathbf{\Delta}_\alpha\} \mathrm{Tr}_{\mathrm{e}} \left[\prod_{\alpha=1}^{N} \left(\mathbf{q}_\alpha + \frac{\mathbf{\Delta}_\alpha}{2}\right) \otimes \left(\mathbf{q}_\alpha - \frac{\mathbf{\Delta}_\alpha}{2}\right)^{\mathrm{T}} \right] \times e^{-\frac{1}{\hbar}\sum_{\alpha=1}^{N}\left(\frac{1}{4}\mathbf{\Delta}_\alpha^{\mathrm{T}}\mathbf{\Delta}_\alpha + \mathbf{q}_\alpha^{\mathrm{T}}\mathbf{q}_\alpha - i\mathbf{p}_\alpha^{\mathrm{T}}\mathbf{\Delta}_\alpha\right)}. \tag{A6}$$

Analytically performing the integration over $\mathbf{\Delta}_\alpha$ (a Gaussian integral), we obtain the final expression in Eq. (15). A similar derivation procedure is used in the previous work of MV-RPMD[71] as well as in the recently derived exact mapping variable Liouvillian.[69]

In state-dependent RPMD approaches, the number of beads N is treated as a convergence parameter.[68,70,72] Recent investigations of NRPMD suggest that a desired numerical convergence can be achieved by using a different number of beads for the electronic mapping variables and the nuclear DOF.[70] In this paper, we use the same N for both the electronic and nuclear DOFs. Figure 4 presents the bead convergence of the NRPMD population dynamics in model II. The numerical results of NRPMD converge at $N = 16$ compared to those obtained from $N = 32$ beads (not shown).

APPENDIX B: THERMOSTATTED NRPMD (T-NRPMD)

In this appendix, we investigate the effect of thermostatting nuclear ring polymer on the NRPMD nonadiabatic dynamics. It is known that ring polymer quantization often introduces spurious frequencies in the RPMD dynamics due to the presence of the high-frequency normal mode vibrations[57] and causes the "spurious resonance problem" for computing spectra[90,119,120] and introducing incorrect frequency in time-correlation functions for nonlinear operators.[120] Thus, the success of any RPMD-type approach relies on the separation of the time scale between the high-frequency normal mode vibrations of the ring polymer and the dynamics of physical interest.[57] Various thermostatted RPMD (TRPMD) approaches[90,119] are proposed to achieve this.[90,119]

Based on the Matsubara dynamics framework, it is shown that this frequency contamination arises due to discarding the imaginary term of the Matsubara Liouvillian.[87,88] This formal analysis[120] shows that TRPMD can be justified by *replacing* the imaginary Matsubara Liouvillian with a friction term, such as the Fokker-Planck operator,[134–136] instead of just discarding the imaginary part of the Matsubara Liouvillian as done in RPMD. Here, we apply a Langevin thermostat that couples to the nuclear normal mode in NRPMD. We first briefly introduce the normal mode representation of the ring polymer before we provide the equation of motion for the thermostatting.

The free ring-polymer Hamiltonian [see Eq. (3) and below] is defined as follows:

$$H_{\mathrm{rp}} = \sum_{\alpha=1}^{N} \frac{\mathbf{P}_\alpha^2}{2\mathbf{M}} + \frac{\mathbf{M}}{2\beta_N^2\hbar^2}(\mathbf{R}_\alpha - R_{\alpha-1})^2. \tag{B1}$$

Often, the dynamical propagation of RPMD (and PIMD) can be simplified by transforming $H_{\rm rp}$ from the above bead representation (or the so-called primitive nuclear coordinate) to the normal mode representation, which is the eigenstate of the Hessian matrix of $H_{\rm rp}$. Diagonalizing the Hessian matrix of $H_{\rm rp}$ provides the eigenvalue, i.e., the following normal mode frequency:

$$\widetilde{\omega}_\mu = \frac{2}{\beta_N \hbar} \sin\left(\frac{\mu\pi}{N}\right), \tag{B2}$$

where $\mu \in [0, N-1]$ represents the index of the normal mode. The same diagonalization process also gives the eigenvector $T_{\alpha\mu}$ of the Hessian matrix, which provides the relation between the primitive coordinate $\{\mathbf{R}_\alpha\}$ and the normal mode coordinate $\{\widetilde{\mathbf{R}}_\mu\}$, as well as the corresponding relation for momenta under two representations. These relations are expressed as follows:

$$\widetilde{\mathbf{R}}_\mu = \sum_{\alpha=1}^{N} \mathbf{R}_\alpha T_{\alpha\mu}; \quad \widetilde{\mathbf{P}}_\mu = \sum_{\alpha=1}^{N} \mathbf{P}_\alpha T_{\alpha\mu}, \tag{B3}$$

$$\mathbf{R}_\alpha = \sum_{\mu=0}^{N-1} T_{\alpha\mu} \widetilde{\mathbf{R}}_\mu, \quad \mathbf{P}_\alpha = \sum_{\mu=0}^{N-1} T_{\alpha\mu} \widetilde{\mathbf{P}}_\mu. \tag{B4}$$

The above transformation matrix elements have the following values:

$$T_{\alpha\mu} = \begin{cases} \sqrt{1/N} & (\mu = 0) \\ \sqrt{2/N}\cos(2\pi\alpha\mu/N) & (1 \le \mu \le \frac{N}{2} - 1) \\ \sqrt{1/N}(-1)^\alpha & (\mu = \frac{N}{2}) \\ \sqrt{2/N}\sin(2\pi\alpha\mu/N) & (\frac{N}{2} + 1 \le \mu \le N - 1). \end{cases} \tag{B5}$$

Under the normal mode representation, the free ring polymer Hamiltonian $H_{\rm rp}$ in Eq. (B1) becomes

$$H_{\rm rp} = \sum_{\mu=0}^{N-1} \frac{\widetilde{\mathbf{P}}_\mu^2}{2\mathbf{M}} + \frac{1}{2}\mathbf{M}\widetilde{\omega}_\mu^2 \widetilde{\mathbf{R}}_\mu^2, \tag{B6}$$

where the normal mode frequency $\widetilde{\omega}_\mu$ is described in Eq. (B2). Note that the interbead coupling terms of the ring polymer become a set of simple quadratic terms with the normal mode frequencies. The NRPMD nuclear equation of motion of described in Eq. (17) under the normal mode representation is expressed as follows:

$$\dot{\widetilde{\mathbf{P}}}_\mu = -\nabla_{\widetilde{\mathbf{R}}_\mu} H_N(\{\mathbf{R}_\alpha\}) = -\sum_\alpha \nabla_{\mathbf{R}_\alpha} H_N(\{\mathbf{R}_\alpha\}) \frac{\partial \mathbf{R}_\alpha}{\partial \widetilde{\mathbf{R}}_\mu}, \tag{B7}$$

where simple chain rule is used to establish the last equality, $-\nabla_{\mathbf{R}_\alpha} H_N(\{\mathbf{R}_\alpha\}) = \dot{\mathbf{P}}_\alpha$ is the nuclear force in Eq. (17), and $T_{\alpha\mu} = \partial\mathbf{R}_\alpha/\partial\widetilde{\mathbf{R}}_\mu$ is the Jacobian matrix element of the transformation between the primitive nuclear variables $\{\mathbf{R}_\alpha\}$ and the normal mode coordinates $\{\widetilde{\mathbf{R}}_\mu\}$ described in Eq. (B4). Note that $T_{\alpha\mu}$ is the same for all $\mathcal{F}$ nuclear DOFs.

The normal mode NRPMD nuclear force $-\nabla_{\widetilde{\mathbf{R}}_\mu} H_N(\{\mathbf{R}_\alpha\})$ in Eq. (B7) contains three types of terms: (i) the force contribution from the free ring polymer, $-\mathbf{M}\omega_\mu^2\widetilde{\mathbf{R}}_\mu$, (ii) the state independent force, $-\sum_\alpha \nabla_{\mathbf{R}_\alpha} V_0(\mathbf{R}_\alpha) T_{\alpha\mu}$, and (iii) the state dependent force, $-\frac{1}{2\hbar}\sum_\alpha \sum_{nm} \nabla_{\mathbf{R}_\alpha} V_{nm}(\mathbf{R}_\alpha)\left([\mathbf{q}_\alpha]_n[\mathbf{q}_\alpha]_m + [\mathbf{p}_\alpha]_n[\mathbf{p}_\alpha]_m - \delta_{nm}\hbar\right) T_{\alpha\mu}$.

Following the previous work of TRPMD,[90,120] the nuclear ring polymer normal mode $\{\widetilde{\mathbf{R}}_\mu\}$ in H_N is coupled to an Langevin thermostat, giving a method that is referred to as the Thermostatted NRPMD (T-NRPMD). In T-NRPMD, the mapping equations of motion remain the same as described in Eq. (18), whereas the nuclear equation of motion in Eq. (B7) is replaced[90,120] by the following one:

$$\dot{\widetilde{\mathbf{P}}}_\mu = -\nabla_{\widetilde{\mathbf{R}}_\mu} H_N(\{\mathbf{R}_\alpha\}) - \boldsymbol{\eta}_\mu \widetilde{\mathbf{P}}_\mu + \sqrt{\frac{2\mathbf{M}\boldsymbol{\eta}_\mu}{\beta_N}}\boldsymbol{\xi}_\mu(t). \tag{B8}$$

The first term is the force from the NRPMD Hamiltonian [Eq. (B7)], the second term is the friction force acting on $\widetilde{\mathbf{P}}_\mu$, with $\boldsymbol{\eta}_\mu$ being the bead-specific normal mode friction matrix, and the last term is the random force, with $\boldsymbol{\xi}_\mu(t)$ representing an uncorrelated, Gaussian-distributed random force[90] with unit variance $\langle\boldsymbol{\xi}_\mu(0)\boldsymbol{\xi}_\mu(t)\rangle = \delta(t)$, and zero mean $\langle\boldsymbol{\xi}_\mu(t)\rangle = 0$. Based on the recent analysis of TRPMD from the Matsubara dynamics framework,[120] we choose the same friction constant for all $\mathcal{F}$ nuclear DOFs associated with the $\mu_{\rm th}$ normal mode, with the μ-specific friction term, $\eta_\mu = 2\lambda|\widetilde{\omega}_\mu|$, where λ is viewed as a parameter.[120] The Langevin equation can be numerically propagated based on the algorithm in previous works,[90,134] whereas the mapping equation of motion is integrated with a symplectic integrator.[109,110]

Figure 5 presents the results of model II obtained from T-NRPMD. Here, we investigate the effects of nuclear thermostatting on the excited state nonadiabatic dynamics and explore the

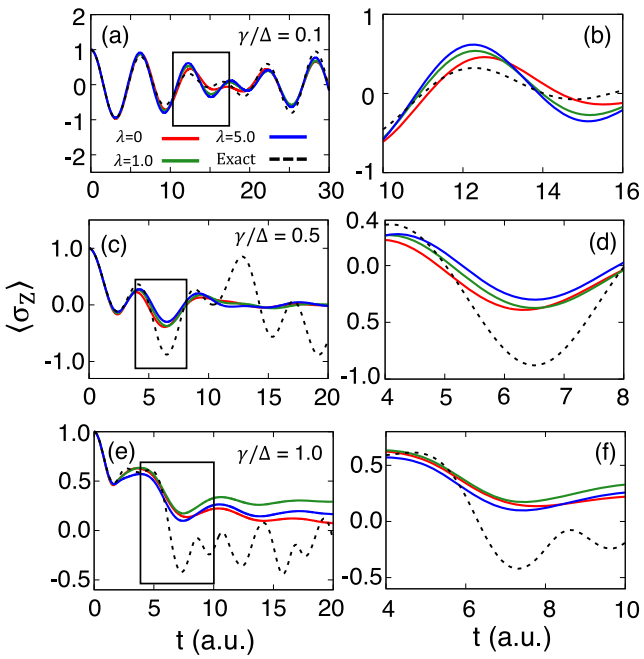

FIG. 5. Population dynamics of model II. (a), (c), and (e) show $\langle\sigma_Z\rangle$ with various electron-phonon coupling strengths, and (b), (d), and (f) depict the magnified plots that correspond to the square regions in the left column. Results are obtained from T-NRPMD with different friction parameters, $\lambda = 0$ (red), $\lambda = 1$ (green), $\lambda = 5$ (blue), as well as the numerical exact results (black dashed line).

impact of various friction constants λ on the population dynamics. The results are obtained by using $\lambda = 0$ (red), i.e., the NRPMD approach (same as results shown in Fig. 3), $\lambda = 1.0$ (green), and $\lambda = 5.0$ (blue), together with the numerically exact results (black dashed lines). Despite that NRPMD provides more accurate population dynamics compared to classical Wigner based methods as discussed in Fig. 3, the population tends to oscillate with a slightly shifted frequency compared to the electronic Rabi frequency. This can be clearly seen by comparing the results of NRPMD (red) and the exact ones (black) in (b), (d), and (f) which depict the magnified plots corresponding to the square regions in (a), (c), and (e). The higher frequency normal modes of the nuclear ring polymer might be the source of these spurious oscillations,[120] which has shown to contaminate the nuclear dynamics.[120]

Using $\lambda = 1.0$ (green), T-NRPMD recovers the correct oscillation frequencies of the electronic population. This value of λ is chosen based on a friction parameter that is derived from achieving the correct nuclear oscillation frequency in a harmonic potential.[120] By recovering the correct nuclear oscillations of R, the coupled electronic dynamics is also improved. We also observed that by applying a small friction parameter $0.5 \leq \lambda \leq 1$, T-NRPMD already improves the dynamics and recovers the correct oscillation period. The population dynamics continues to oscillate with the correct frequency when further increasing the friction parameter to the overdamped regime with $\lambda = 5.0$ (solid blue line). The correct electronic oscillation is likely stemmed from the correct nuclear oscillations when applying thermostat which has been demonstrated in the previous work.[120]

These investigations demonstrate that T-NRPMD is a valuable tool for providing accurate excited state dynamics and alleviate the spurious frequency problem associated with the ring polymer quantization. Future studies include rigorous derivation of the T-NRPMD approach through the Matsubara dynamics framework[87,88] with the mapping Liouvillian[69] to treat electronic states explicitly.

REFERENCES

[1] J. C. Tully, J. Chem. Phys. **137**, 22A301 (2012).
[2] R. Kapral, J. Phys.: Condens. Matter **27**, 073201 (2015).
[3] H.-P. Breuer and F. Petruccione, *The Theory of Open Quantum Systems* (Oxford University Press, 2002).
[4] A. Ishizaki and Y. Tanimura, J. Phys. Soc. Jpn. **74**, 3131 (2005).
[5] Y. Tanimura, J. Phys. Soc. Jpn. **75**, 082001 (2006).
[6] L. Chen, R. Zheng, Q. Shi, and Y. Yan, J. Chem. Phys. **131**, 094502 (2009).
[7] J. Strumpfer and K. Schulten, J. Chem. Theory Comput. **8**, 2808 (2012).
[8] N. Makri and D. E. Makarov, J. Chem. Phys. **102**, 4600 (1995).
[9] N. Makri and D. E. Makarov, J. Chem. Phys. **102**, 4611 (1995).
[10] A. Strathearn, P. Kirton, D. Kilda, J. Keeling, and B. W. Lovett, Nat. Commun. **9**, 3322 (2018).
[11] H. Meyer, U. Manthe, and L. Cederbaum, Chem. Phys. Lett. **165**, 73 (1990).
[12] M. Beck, A. Jackle, G. Worth, and H. Meyer, Phys. Rep. **324**, 1 (2000).
[13] H. Wang and M. Thoss, J. Chem. Phys. **119**, 1289 (2003).
[14] P. Eisenbrandt, M. Ruckenbauer, S. Römer, and I. Burghardt, J. Chem. Phys. **149**, 174101 (2018).
[15] G. W. Richings and S. Habershon, J. Chem. Phys. **148**, 134116 (2018).
[16] D. Makhov, W. Glover, T. Martinez, and D. Shalashilin, J. Chem. Phys. **141**, 054110 (2014).
[17] B. F. E. Curchod and T. J. Martinez, Chem. Rev. **118**, 3305 (2018).
[18] P. L. Walters and N. Makri, J. Chem. Phys. **144**, 044108 (2016).
[19] P. L. Walters and N. Makri, J. Phys. Chem. Lett. **6**, 4959 (2015).
[20] S. M. Greene and V. S. Batista, J. Chem. Theory Comput. **13**, 4034 (2017).
[21] J. Ren, Z. Shuai, and G. Chan, J. Chem. Theory Comput. **14**, 5027 (2018).
[22] W. H. Miller, J. Phys. Chem. A **113**, 1405 (2009).
[23] J. Tully, J. Chem. Phys. **93**, 1061 (1990).
[24] J. E. Subotnik, A. Jain, B. Landry, A. Petit, W. Ouyang, and N. Bellonzi, Annu. Rev. Phys. Chem. **67**, 387 (2016).
[25] L. Wang, A. Akimov, and O. V. Prezhdo, J. Phys. Chem. Lett. **7**, 2100 (2016).
[26] R. Crespo-Otero and M. Barbatti, Chem. Rev. **118**, 7026 (2018).
[27] W. H. Miller, J. Phys. Chem. A **105**, 2942 (2001).
[28] X. Sun, H. Wang, and W. H. Miller, J. Chem. Phys. **109**, 7064 (1998).
[29] Q. Shi and E. Geva, J. Phys. Chem. A **108**, 6109 (2004).
[30] S. Bonella and D. Coker, J. Chem. Phys. **122**, 194102 (2005).
[31] N. Makri, Phys. Chem. Chem. Phys. **13**, 14442 (2011).
[32] P. Huo and D. F. Coker, J. Chem. Phys. **135**, 201101 (2011).
[33] M. Lee, P. Huo, and D. F. Coker, Annu. Rev. Phys. Chem. **67**, 639 (2016).
[34] D. M. Kernan, G. Ciccotti, and R. Kapral, J. Phys. Chem. B **112**, 424 (2008).
[35] H. Kim, A. Nassimi, and R. Kapral, J. Chem. Phys. **129**, 084102 (2008).
[36] C. Hsieh and R. Kapral, J. Chem. Phys. **137**, 22A507 (2012).
[37] C. Hsieh and R. Kapral, J. Chem. Phys. **138**, 134110 (2013).
[38] W. H. Miller and S. J. Cotton, Faraday Discuss. **195**, 9 (2016).
[39] G. Tao, J. Phys. Chem. Lett. **7**, 4335 (2016).
[40] A. A. Kananenka, C.-Y. Hsieh, J. Cao, and E. Geva, J. Phys. Chem. Lett. **9**, 319 (2018).
[41] J. S. Sandoval, A. Mandal, and P. Huo, J. Chem. Phys. **149**, 044115 (2018).
[42] S. J. Cotton and W. H. Miller, J. Chem. Phys. **150**, 104101 (2019).
[43] M.-L. Zhang, B. J. Ka, and E. Geva, J. Chem. Phys. **125**, 044106 (2006).
[44] W. C. Pfalzgraff, A. Kelly, and T. E. Markland, J. Phys. Chem. Lett. **6**, 4743 (2015).
[45] A. Kelly, N. J. Brackbill, and T. E. Markland, J. Chem. Phys. **142**, 094110 (2015).
[46] A. Kelly, A. Montoya-Castillo, L. Wang, and T. E. Markland, J. Chem. Phys. **144**, 184105 (2016).
[47] E. Mulvihill, A. Schubert, X. Sun, B. D. Dunietz, and E. Geva, J. Chem. Phys. **150**, 034101 (2019).
[48] P. V. Parandekar and J. C. Tully, J. Chem. Theo. Comp. **2**, 229 (2006).
[49] J. R. Schmidt, P. V. Parandekar, and J. C. Tully, J. Chem. Phys. **129**, 044104 (2008).
[50] S. Habershon and D. E. Manolopoulos, J. Chem. Phys. **131**, 244518 (2009).
[51] U. Muller and G. Stock, J. Chem. Phys. **111**, 77 (1999).
[52] B. J. Berne and D. Thirumalai, Annu. Rev. Phys. Chem. **37**, 401 (1986).
[53] D. M. Ceperley, Rev. Mod. Phys. **67**, 279 (1995).
[54] D. Chandler and P. G. Wolynes, J. Chem. Phys. **74**, 4078 (1981).
[55] J. Cao and G. Voth, J. Chem. Phys. **100**, 5106 (1994).
[56] S. Jang and G. Voth, J. Chem. Phys. **111**, 2371 (1999).
[57] S. Habershon, D. E. Manolopoulos, T. E. Markland, and T. F. Miller, Annu. Rev. Phys. Chem. **64**, 387 (2013).
[58] I. R. Craig and D. E. Manolopoulos, J. Chem. Phys. **121**, 3368 (2004).
[59] A. R. Menzeleev, N. Ananth, and T. F. Miller, J. Chem. Phys. **132**, 034106 (2010).
[60] A. R. Menzeleev, N. Ananth, and T. F. Miller, J. Chem. Phys. **135**, 074106 (2011).
[61] J. S. Kretchmer and T. F. Miller, J. Chem. Phys. **138**, 134109 (2013).
[62] J. Kretchmer and T. F. Miller, Inorg. Chem. **55**, 1022 (2016).
[63] R. L. Kenion and N. Ananth, Phys. Chem. Chem. Phys. **18**, 26117 (2016).
[64] R. F. N. Boekelheide and T. F. Miller, Proc. Natl. Acad. Sci. U. S. A. **108**, 16159 (2011).
[65] S. L. Wang, S. D. Fried, and T. E. Markland, Proc. Natl. Acad. Sci. U. S. A. **111**, 18454 (2014).
[66] O. Marsalek and T. E. Markland, J. Phys. Chem. Lett. **8**, 1545 (2017).
[67] T. E. Markland and M. Ceriotti, Nature Rev. Chem. **2**, 0109 (2018).
[68] J. O. Richardson and M. Thoss, J. Chem. Phys. **139**, 031102 (2013).
[69] T. J. H. Hele and N. Ananth, Faraday Discuss. **195**, 269 (2016).

[70]J. O. Richardson, P. Meyer, M.-O. Pleinert, and M. Thoss, Chem. Phys. **482**, 124 (2017).
[71]N. Ananth, J. Chem. Phys. **139**, 124102 (2013).
[72]J. R. Duke and N. Ananth, J. Phys. Chem. Lett. **06**, 4219 (2015).
[73]S. Pierre, J. R. Duke, T. J. H. Hele, and N. Ananth, J. Chem. Phys. **147**, 234103 (2017).
[74]T. Yoshikawa and T. Takayanagi, Chem. Phys. Lett. **564**, 1 (2013).
[75]A. R. Menzeleev, F. Bell, and T. F. Miller, J. Chem. Phys. **140**, 064103 (2014).
[76]J. Kretchmer, N. Boekelheide, J. F. Warren, J. R. Winkler, H. B. Gray, and T. F. Miller, Proc. Natl. Acad. Sci. U. S. A. **115**, 6129 (2018).
[77]S. N. Chowdhury and P. Huo, J. Chem. Phys. **147**, 214109 (2017).
[78]P. Shushkov, R. Li, and J. C. Tully, J. Chem. Phys. **137**, 22A549 (2012).
[79]F. A. Shakib and P. Huo, J. Phys. Chem. Lett. **8**, 3073 (2017).
[80]X. Tao, P. Shushkov, and T. F. Miller, J. Chem. Phys. **148**, 102327 (2018).
[81]X. Tao, P. Shushkov, and T. F. Miller, J. Phys. Chem. A **123**, 3013 (2019).
[82]R. Kaur and R. Welsch, J. Chem. Phys. **150**, 114105 (2019).
[83]H. D. Meyer and W. H. Miller, J. Chem. Phys. **70**, 3214 (1979).
[84]G. Stock and M. Thoss, Phys. Rev. Lett. **78**, 578 (1997).
[85]G. Stock and M. Thoss, Phys. Rev. A **59**, 64 (1999).
[86]R. P. Feynman and A. R. Hibbs, *Quantum Mechanics and Path Integrals* (Dover Publications, Inc., 1965).
[87]T. J. H. Hele, M. J. Willatt, A. Muolo, and S. C. Althorpe, J. Chem. Phys. **142**, 134103 (2015).
[88]T. J. H. Hele, M. J. Willatt, A. Muolo, and S. C. Althorpe, J. Chem. Phys. **142**, 191101 (2015).
[89]R. Welsch, K. Song, Q. Shi, S. C. Althorpe, and T. F. Miller, J. Chem. Phys. **145**, 204118 (2016).
[90]M. Ceriotti, M. Parrinello, T. E. Markland, and D. E. Manolopoulos, J. Chem. Phys. **133**, 124104 (2010).
[91]T. J. H. Hele, "An electronically non-adiabatic generalization of ring polymer molecular dynamics," MChem thesis, Exeter College, University of Oxford, 2011.
[92]J. R. Duke and N. Ananth, Faraday Discuss. **195**, 253 (2016).
[93]M. H. Alexander, Chem. Phys. Lett. **347**, 436 (2001).
[94]J. R. Schmidt and J. C. Tully, J. Chem. Phys. **127**, 094103 (2007).
[95]N. Ananth and T. F. Miller, J. Chem. Phys. **133**, 234103 (2010).
[96]J. Lu and Z. Zhou, J. Chem. Phys. **146**, 154110 (2017).
[97]W. B. Case, Am. J. Phys. **76**, 937 (2008).
[98]E. Wigner, Phys. Rev. **40**, 749 (1932).
[99]M. Hillery, R. O'Connell, M. Scully, and E. Wigner, Phys. Rep. **106**, 121 (1984).
[100]J.-L. Liao and G. A. Voth, J. Phys. Chem. B **106**, 8449 (2002).
[101]S. Bonella and D. Coker, J. Chem. Phys. **118**, 4370 (2003).
[102]E. R. Dunkel, S. Bonella, and D. F. Coker, J. Chem. Phys. **129**, 114106 (2008).
[103]W. H. Miller and S. J. Cotton, J. Chem. Phys. **145**, 081102 (2016).
[104]S. J. Cotton and W. H. Miller, J. Chem. Phys. **145**, 144108 (2016).
[105]S. J. Cotton and W. H. Miller, J. Chem. Phys. **139**, 234112 (2013).
[106]M. A. C. Saller, A. Kelly, and J. O. Richardson, J. Chem. Phys. **150**, 071101 (2019).
[107]E. A. Coronado, J. Xing, and W. H. Miller, Chem. Phys. Lett. **349**, 521 (2001).
[108]S. A. Sato, A. Kelly, and A. Rubio, Phys. Rev. B **97**, 134308 (2018).
[109]A. Kelly, R. van Zon, J. Schofield, and R. Kapral, J. Chem. Phys. **136**, 084101 (2012).
[110]M. S. Church, T. J. H. Hele, G. S. Ezra, and N. Ananth, J. Chem. Phys. **148**, 102326 (2018).
[111]M. E. Tuckerman, B. J. Berne, G. J. Martyna, and M. L. Klein, J. Chem. Phys. **99**, 2796 (1993).
[112]L. H. de la Peña, Mol. Phys. **112**, 929 (2014).
[113]D. T. Colbert and W. H. Miller, J. Chem. Phys. **96**, 1982 (1992).
[114]P. Huo and D. F. Coker, Mol. Phys. **110**, 1035 (2012).
[115]P. Huo and D. F. Coker, J. Chem. Phys. **137**, 22A535 (2012).
[116]S. C. Althorpe, N. Ananth, G. Angulo, R. D. Astumian, V. Beniwal, J. Blumberger, P. G. Bolhuis, B. Ensing, D. R. Glowacki, S. Habershon, S. Hammes-Schiffer, T. J. H. Hele, N. Makri, D. E. Manolopoulos, L. K. McKemmish, T. F. Miller III, W. H. Miller, A. J. Mulholland, T. Nekipelova, E. Pollak, J. O. Richardson, M. Richter, P. R. Chowdhury, D. Shalashilin, and R. Szabla, Faraday Discuss. **195**, 311 (2016).
[117]J. Liu and W. H. Miller, J. Chem. Phys. **134**, 104101 (2011).
[118]A. Poulsen, G. Nyman, and P. J. Rossky, J. Chem. Phys. **119**, 12179 (2003).
[119]M. Rossi, M. Ceriotti, and D. E. Manolopoulos, J. Chem. Phys. **140**, 234116 (2014).
[120]T. J. H. Hele, Mol. Phys. **114**, 1461 (2016).
[121]C. Venkataraman, A. V. Soudackov, and S. Hammes-Schiffer, J. Phys. Chem. C **114**, 487 (2010).
[122]A. Hazra, A. V. Soudackov, and S. Hammes-Schiffer, J. Phys. Chem. B **114**, 12319 (2010).
[123]A. Hazra, A. V. Soudackov, and S. Hammes-Schiffer, J. Phys. Chem. Lett. **2**, 36 (2011).
[124]P. Goyal and S. Hammes-Schiffer, J. Phys. Chem. Lett. **6**, 3515 (2015).
[125]P. Goyal, C. A. Schwerdtfeger, A. V. Soudackov, and S. Hammes-Schiffer, J. Phys. Chem. B **120**, 2407 (2016).
[126]P. Goyal and S. Hammes-Schiffer, ACS Energy Lett. **2**, 512 (2017).
[127]A. Mandal, F. A. Shakib, and P. Huo, J. Chem. Phys. **148**, 244102 (2018).
[128]S. Hammes-Schiffer, J. Am. Chem. Soc. **137**, 8860 (2015).
[129]A. Mandal, J. S. Sandoval, F. A. Shakib, and P. Huo, J. Phys. Chem. A **123**, 2470 (2019).
[130]A. Mandal, S. Yamijala, and P. Huo, J. Chem. Theory Comput. **14**, 1828 (2018).
[131]Q. Shi and E. Geva, J. Chem. Phys. **118**, 7562 (2003).
[132]S. Jang, A. V. Sinitskiy, and G. A. Voth, J. Chem. Phys. **140**, 154103 (2014).
[133]A. N. S. Bonella and R. Kapral, J. Chem. Phys. **133**, 134115 (2010).
[134]G. Bussi and M. Parrinello, Phys. Rev. E. **75**, 056707 (2007).
[135]C. Gardiner, *Handbook of Stochastic Methods*, 3rd ed. (Springer, New York, 2003).
[136]H. Risken, *The Fokker-Planck Equation*, 2nd ed. (Springer, New York, 1989).